FlyEyes: Integrating CCID-35 into PUEO AO system at CFHT

Kevin K.Y. Ho[a], Jean-Charles Cuillandre[a], Chueh-Jen Lin[b], Tom Benedict[a], Olivier Lai[a], Jeff Ward[a], Derrick Salmon[a], Gerry Luppino[c], James Beletic[d], Reinhold Dorn[e], Pascal Puget[f] Barry Burke[g], Shiang-Yu Wang[b],

[a] Canada France Hawaii Telescope, Kamuela, HI, USA
[b] Institute for Astronomy and Astrophysics, National Taiwan University, Taipei, Taiwan, R.O.C.
[c] Institute for Astronomy, University of Hawaii, Honolulu, HI, USA
[d] Rockwell Scientific Company, Thousand Oaks, CA , USA
[e] European Southern Observatory, Garching, Germany
[f]Observatoire de Paris, Meudon, France
[g] MIT Lincoln Labs, Lexington, MA, USA

ABSTRACT

A project to upgrade PUEO, the CFHT AO system, was first proposed in 2002. As part of the upgrade effort, a technology project was conceived to evaluate and characterize the backside-illuminated CCID-35 detector as suitable a replacement for the array of avalanche photo diode modules (APDs) in the curvature wavefront sensor. The CCID-35 was envisioned to replace an array of expensive APDs thus providing a cost-effective means of upgrading PUEO to a higher-order system. Work on the project, dubbed FlyEyes, occurred sporadically until Oct 2005 but substantial progress has been made since. This paper was intended to report on the performance of FlyEyes in PUEO but unfortunately the instrument was not ready for tests at the time of this writing. This paper summarizes the progress made on the project thus far and touches upon some of the difficulties encountered.

Keywords: CCD, adaptive optics, wavefront sensing

1. INTRODUCITON

The CFHT adaptive optics system, PUEO, has been in service since first light in 1996 and continues to see significant usage. PUEO is based on curvature wavefront sensing with a 19-element bimorph deformable mirror (DM) and 19 passively quenched APDs. Light from the wavefront is divided into 19 subpupils by a lenslet array and fed via optical fibers to the APDs, which do the photon counting. FlyEyes replaces the APDs with two CCID-35 detectors and an SDSU II controller. The optical fibers are removed from the APDs and rerouted to the CCID-35s.

Figure 1 shows a block diagram of PUEO and highlights where the CCID-35s integrates into PUEO. A more detailed explanation of FlyEyes concept is given in papers by K.Ho et al (1) and J.C. Cuillandre et al (2). Much of the work on CCID-35 was drawn from previous work done by R.Dorn (3) and J.Beletic et al (4).

The first stage of FlyEyes is complete. The cryostat for the CCID-35s is fully assembled. The detectors operates at –100 C. Dark current is not much of a concern since the exposure time is less than 4 msec. The surface of the fiber bundle is positioned approximately 200 μm off the surface of the detector. Extreme care was taken during the alignment process so as not to damage the chip or the bond wires. A new fiber bundle had to be made since the first bundle was severely damaged during the assembly process. Although it set the schedule back a few weeks, it presented the opportunity to improve upon the fiber bundle design and assembly process. The final fiber bundle is more robust and was much easier to assemble than the first.

First light in image mode was achieved in the early part of January. Gain and noise were characterized. This was somewhat difficult since the classical means of using flat fields across the detector was not feasible. Gain and noise

measurements were done after the fibers had been positioned so the only light path was through the fibers. Since the fiber bundle sits so close to the detector there is no other way of getting light onto the detector except through the fibers. In hindsight, gain and noise characterization should have been done prior to installing the fibers. A window could have been installed to provide a port for the light. Removing the fiber bundle for characterization was considered but ruled out due to the risk of potentially damaging the fiber bundle or CCD.

Quite a bit of work remains before any on-sky tests with FlyEyes and PUEO. Work on DSP code on the AO mode for the SDSU II continues. The electronic interface board, which transfers the intensity data from the SDSU to the AO real-time computer needs to be assembled and tested. At the heart of the board are two Lattice field programmable gate arrays. These devices provide tremendous flexibility in tweaking the design during the test and integration. Final integration with PUEO is slated occur in the next couple of months.

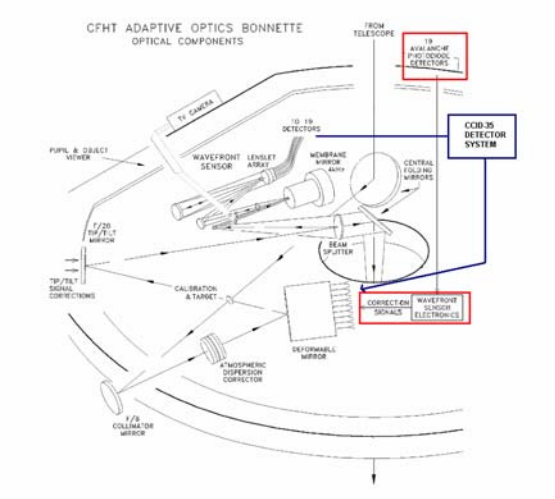

Figure 1 FlyEyes location in PUEO.

2. FLYEYES FIBER BUNDLE

2.1. Constraints and Design

For the purposes of initial testing, FlyEyes was made to be plug-compatible with the existing APDs. This constrained the choice of fiber and total number of fibers in the system.

The fiber used was the same used in the original AO system, a silica/silica fiber with a 100µm diameter core, 120µm diameter clad, a 140µm diameter polyamide mechanical reference layer, and a 240µm diameter acrylate abrasion layer. The choice in materials meant that many of the conventional fiber termination tools could not be used, and special tooling was required.

The CCID-35 supports up to 80 fibers. Since the existing AO system has only 19 channels, populating all 80 fibers was viewed as overkill, and a 54-fiber bundle was designed and fabricated.

Outside the cryostat, the vacuum feed-through was designed with individual holes for each fiber and provision to anchor a conventional fiber jacket around each one. This made for a robust arrangement on the outside of the cryostat, but caused issues during construction that will be discussed later.

Inside the cryostat, in order to get a spot size that would fit within a superpixel, the fiber bundle had to be positioned between 1 and 320µm above the face of the CCID-35, and centered to within a few tens of microns in X and Y, with the

centering tolerances getting tighter as the height above the CCD increased. The goal was 200μm height, which would give about +/- 80μm positioning tolerance in X and Y.

FlyEyes was designed with an X-Y-θ adjustment mechanism for each of the two fiber bundles that would be installed in front of the two CCID-35. Only one fiber bundle was installed. The range of motion of the adjustment mechanism provided for +/- 0.6 to 0.7mm in X and Y, and several degrees in rotation. There was no provision for adjustment in Z, or the height of the bundle above the face of the CCD. This had to be designed into the fiber bundle itself.

The superpixels on the CCID-35 have a center-to-center spacing of 550μm in X and 360μm in Y. To arrange the fibers in this grid, silicon v-groove blocks were used in a stack. See Figure 2. The stack was assembled dry and potted with epoxy.

The greatest risk with the fiber bundle, aside from contact with the CCD face, was possible collision with bond wires. Metrology of the two CCID-35s showed the highest bond wire to be on the order of 720μm higher than the face of the CCD. Rather than design around individual bond wires, this height was assumed for all bond wires. The mechanical support for the fiber bundle was designed so that the bundle could not collide with the bond wires regardless of the position of the adjustment mechanism. Figure 4 shows a computer generated rendering of the fiber bundle nominally positioned over the face of the CCD.

2.2. Construction

Construction began with the silicon v-groove stack, using an alignment tool designed for the purpose. See Figure 3 and 5. Tra-Bond F113 epoxy was used to pot the v-groove stack and to attach it to its mechanical support. The choice of epoxy was driven by the need for good wicking characteristics and a final hardness that allowed for optical polishing.

The bundle was then ground to length and polished. See Figure 6. The target height during polishing was 200μm above the CCID-35 face, but the grinding operation was stopped at 183μm to leave room for final polish.

The vacuum feed-through was then populated and potted with Stycast 2850 FT epoxy. The fiber bundle was tested for leaks at this stage. Aside from the expected water absorption and the remaining volatiles from the epoxies, the feed-through had no leaks.

Finally, the outside ends of the fibers were terminated with FC connectors, making it plug-compatible with the existing APDs in place on PUEO.

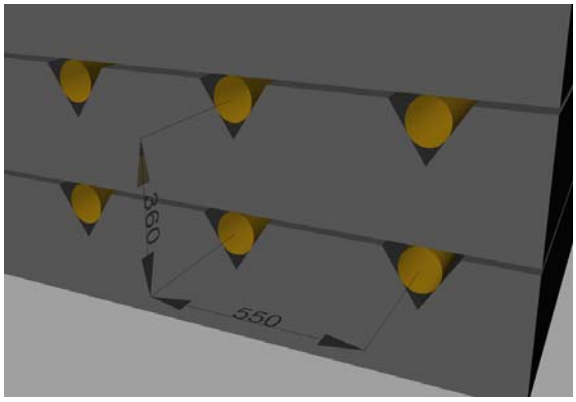

Figure 2 Silicon v-grooves.

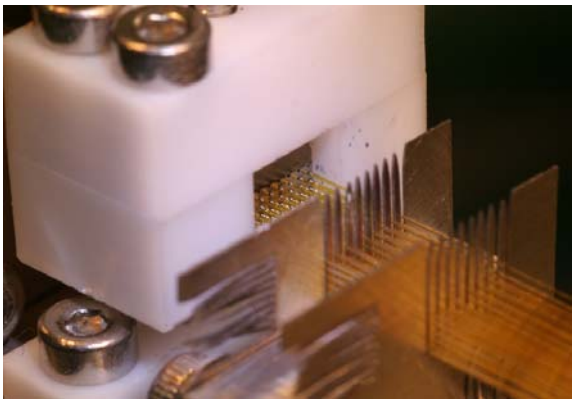

Figure 3 Fiber alignment tool.

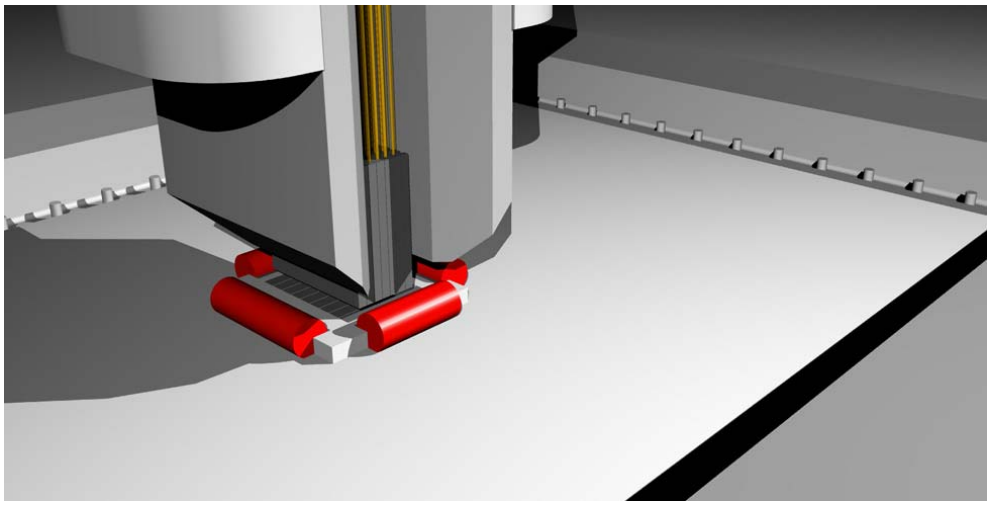

Figure 4 Fiber bundle positioned above the CCID-35. The red tubes depict the bond wires.

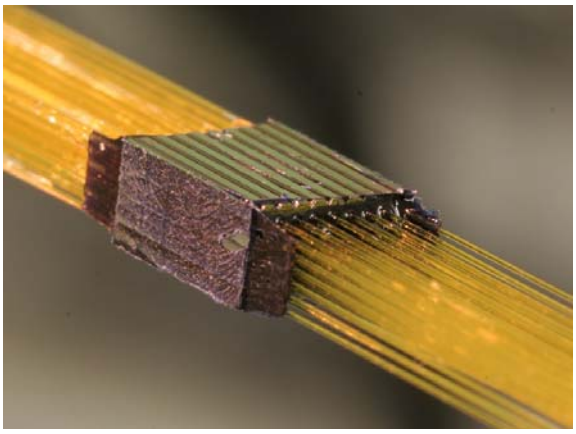

Figure 5 Fibers during assembly.

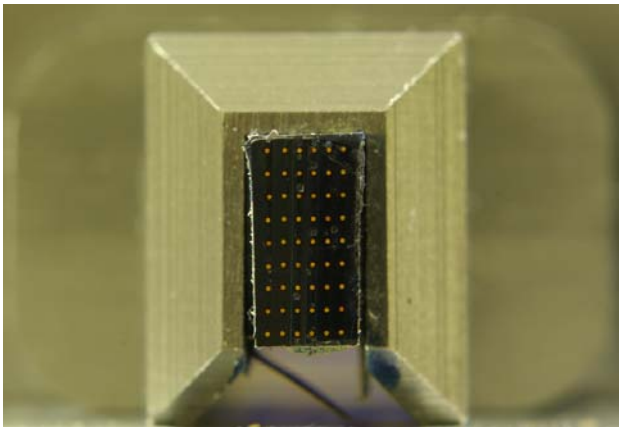

Figure 6 End view of fiber bundle.

2.3. Installation and Alignment

The fiber bundle was installed with the CCID-35 operating at room temperature in imaging mode. Light was injected into the fibers, and the CCD was read out in real-time to provide a streaming video image of the fiber spots. The fiber spots on the CCD are shown in Figure 7. A picture of a frontside illuminated CCID-35 die is shown for comparison in Figure 8.

Because there was no way of knowing the alignment of the fiber bundle to the CCD other than through the CCD image itself, a fair amount of caution was used during initial installation. X, Y, and θ were controlled using the adjustment mechanism in the camera. Z was controlled using a stack of shims that were removed, one at a time, to lower the bundle toward the face of the CCD in a controlled fashion.

In the end the estimated height of the bundle above the CCD face was close to the 183μm estimated at the end of the grinding phase, and the spots were centered in the super pixels. During alignment the bundle was removed and installed several times with no apparent shift in Z.

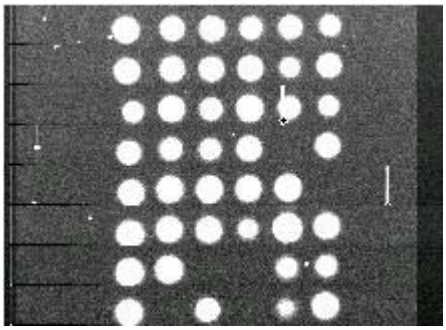

Figure 7 Fiber spots on CCID-35.

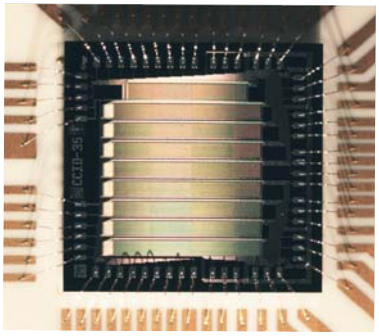

Figure 8 CCID-35 die.

2.4. Drawbacks and Plans for a New Bundle

By far the biggest drawback in the design of the fiber bundle was the vacuum feed-through. By necessity, bare fibers had to be used in vacuum and jacketed fibers outside the cryostat. This made for a fiber bundle with a very heavy and fragile end. Several fibers were broken during fabrication and installation because of this as can be seen in Figure 7. The missing spots show the location of the broken or poor transmission fibers. Also evident in the figure are the defects in the detector.

During the course of testing, it was found that the bare fibers could be made into a robust, yet flexible structure, if they were twisted into a rope. If each fiber is allowed to rotate freely while the twisting is being done, the fibers naturally lay against each other without any tendency for the rope to unwind. This arrangement has not been tested for potential optical losses, but if tests along those lines give promising results, future bundles will be designed with this idea in mind.

Another problem encountered while assembling the v-groove stack was the alignment of the individual silicon v-groove blocks, which proved to be difficult. The existing fiber bundle was aligned by registering the cleaved edges of the v-groove blocks. This was less than ideal since the cleaved edges of the v-groove blocks were not consistent one to the next, resulting in shifts in fiber position from one row to the next. This can be seen in Figure 7 where some spots extend beyond the column boundary. A better arrangement would be to register off the fibers themselves, though tooling for doing this has not yet been developed.

3. GAIN AND NOISE CHARACTERIZATION

The standard transfer curve method uses flat field images to determine the gain and noise performance of a CCD imaging system. For FlyEyes, a flat field could be not achieved since the fiber bundle had been inserted before characterization. Another approach was developed to derive the transfer curve.

A small sub-region (20x20 pixels) around each spot was selected. Figure 9 shows the intensity profile of one spot. A stable light source was tuned to saturate a few pixels at the peak. Roughly 400 images at a fixed exposure time were taken. The mean and standard deviation (or, variance) of each single pixel, on a pixel-by-pixel basis, in the sub-region were calculated. The data was fitted using the following formula.

$$\sigma_S = \sqrt{\frac{S}{g} + (e_{err} S)^2 + \sigma_{read}^2} \tag{3.1}$$

where σ_S - standard deviation of the signal level,
S - mean signal level in ADUs,
g - gain,
σ_{read} - read noise,
e_{err} - coefficient due to other noise source.

The $(e_{err}S)^2$ term in standard transfer curve method typically represents the nonuniformity of pixel sensitivity resulting from the fabrication of CCD or fixed-pattern noise. However, in the method described above, the dominant contributor is the distribution of exposure time. Hundreds of images are taken for the calculation and the deviation of exposure time from nominal must be taken into account. The term was more prevalent at lower exposure times and as expected, reduced at longer exposure time.

Figure 10 shows the resultant photon transfer curve from this method. The read and shot noise domains follow the standard photon transfer curve.

There are eight output amplifiers on the CCID-35, each driving a column on the CCD. They feed into individual video channels in the SDSU II. The drain voltages of the output amplifiers, which are individually programmable, were stepped through a reasonable range to determine the best bias level to achieve the lowest noise performance. The read noise was quite the same within 19.8V to 20.2 V – 20.0 V was selected as the optimal operating point for all the amplifiers. The read noise varied from a low of 1.8 e- to 2.6 e-, which was slightly higher than the goal of 2.0 e-. R. Dorn (2) achieved < 1.5 e- noise performance with a frontside illuminated version of the CCID-35. A slightly higher noise was expected since the FlyEyes CCID-35 is a backside illuminated device. Perhaps the noise could be reduced by improving the shielding of the wires and grounding of the detector system or tweaking the timing but not much effort has been put forth to do so at this time. Figures 11 and 12 show the noise and gain of all eight columns of the CCD through the corresponding amplifier channels.

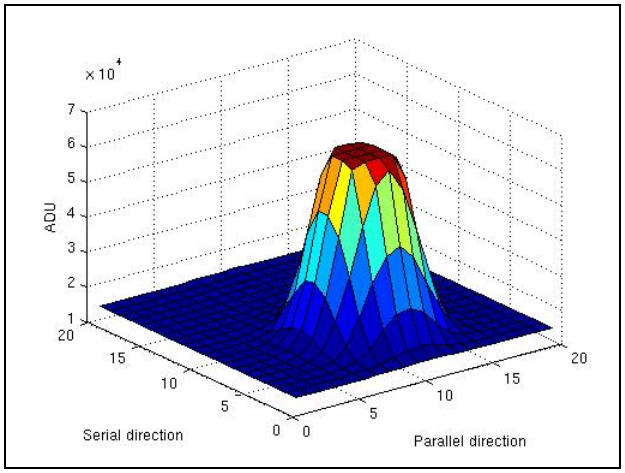

Figure 9 Distribution of intensity of one spot.

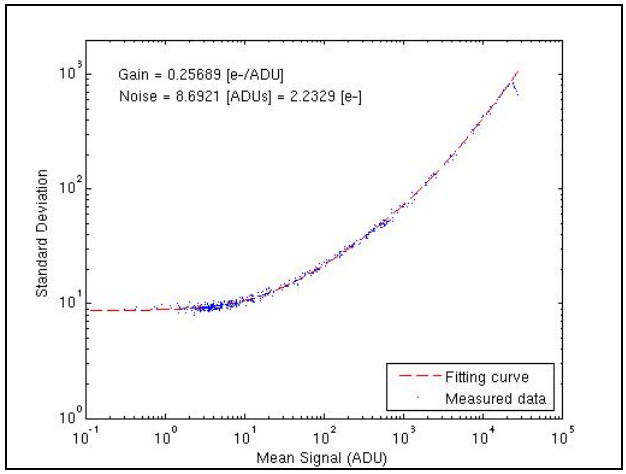

Figure 10 Typical transfer curve.

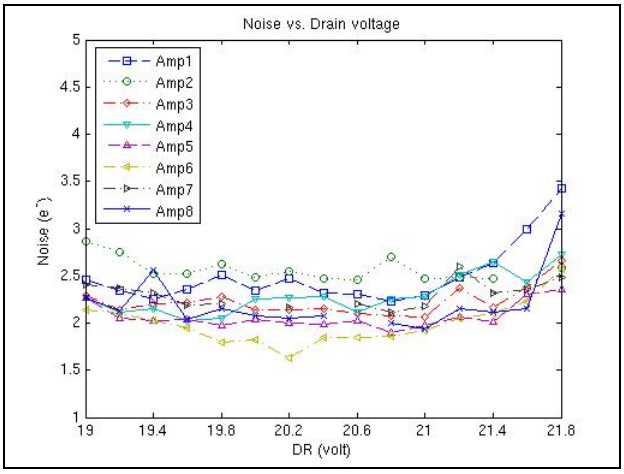

Figure 11 Noise vs drain voltage for 8 amplifier channels.

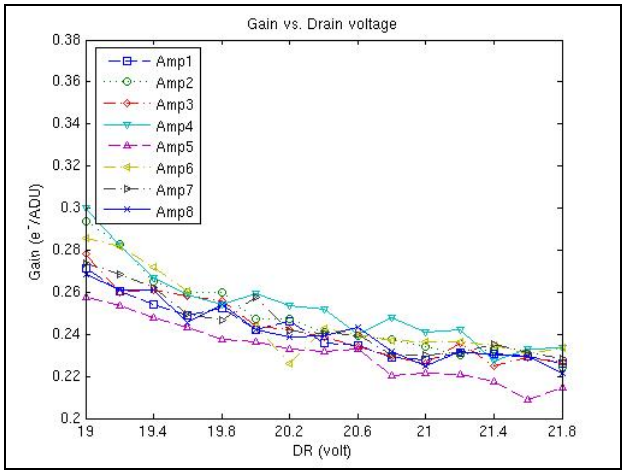

Figure 12 Gain vs drain voltage for 8 amplifier channels.

4. SIMULATIONS

Simulations comparing the wavefront sensor (WFS) measurement variance and the corresponding Strehl attenuation between APDs and the CCID-35 are presented. The formulas used for the simulations in the case of the CCID-35 are valid for Shack-Hartman wavefront sensors and were adopted here to illustrate qualitatively the comparative performance between the CCID-35 and APDs. The APD parameter values used for the calculations were read noise of 0 e- read noise and quantum efficiency (QE) of 0.4. The measured read noise of 1.8 e- and QE of 0.9 were used for the CCID-35. Figure 13 shows two pairs of the WFS measurement variance and Strehl attenuation - one set is plotted against photons and the other against magnitude. The solid lines are those of the APD and dotted lines those of the CCID-35 at three different exposure times of 1, 2 and 4 msec (1 kHz, 500 Hz, 250 Hz).

Photon noise dominates with the APD. The equation to calculate the WFS measurement variance is:

$$\sigma_{WFS}^{\ 2} = \frac{7.2}{N_{photon} * QE_{APD}} \quad (\text{rad}^2) \tag{4.1}$$

where N_{photon} - number of photons,

QE_{APD} =0.4 - APD quantum efficiency.

The equations for the CCID-35 are:

$$\sigma_{WFS}^{\ 2} = \frac{\frac{\pi^4}{3} * (\sigma_{read} * n_{pixels})^2}{(N_{photon} * QE_{CCD})^2} + \sigma_{bandwidth}^{\ 2} \quad (\text{rad}^2) \tag{4.2}$$

where σ_{read} = 1.8 e- - read noise (e-) ,

n_{pixels} = 4 - number of pixels for detection ,

N_{photon} - number of photons,

QE_{CCD} =0.9 - CCID-35 quantum efficiency,

$\sigma_{bandwidth}^{\ 2}$ = 0 (1 kHz) - phase lag error (radians^2).

Increasing the exposure time at high magnitudes improves the WFS measurement variance by increasing the SNR but at a cost of reducing the control loop bandwidth. The reduced bandwidth adds a phase lag error given by equation 4.3. The two dotted curves show σ_{WFS} with exposure times of 2 msec (500 Hz) and 4 msec (250 Hz) with σ_{error} of 0.2 and 0.8 added respectively. For Mauna Kea, the Greenwood frequency is 21 Hz. The F_{3db} is assumed to be 1/10 of the exposure frequency.

The phase lag error is given by:

$$\sigma_{bandwidth}{}^2 = \left(\frac{F_{Greenwood}}{F_{3db}}\right)^{\frac{5}{3}} \quad (\text{rad}^2) \tag{4.3}$$

where $F_{Greenwood}$ - atmospheric turbulence bandwidth (Hz),

F_{3db} - AO loop bandwidth (Hz).

The Greenwood frequency, which determines the bandwidth necessary to reject phase fluctuations in a close-loop AO system, is computed by:

$$F_{Greenwood} = \frac{0.427 * v}{r_0} \quad (\text{Hz}) \tag{4.4}$$

where v = 10 m/sec - mean wind speed,

r_0 = 0.2 m - coherence length.

The advantage of APDs over the CCID-35 is the absence of read noise, where the CCID-35 gains is in QE. At high flux levels up to 12.5 magnitude, the CCID-35 should perform better than the APDs– lower Strehl attenuation. At low flux where read noise becomes significant, the reverse is true but increasing the CCID-35 exposure time helps improve the WFS measurement variance. In PUEO, the integration time of the APDs is fixed at 1 KHz but there are provisions for adjustment. The strategy using the CCID-35 is to lengthen the exposure time and modify the AO close loop bandwidth at the lower flux levels.

5. SUMMARY

The greatest technical challenge has been the fabrication of the fiber bundle. The current fiber bundle is not ideal but suitable for the first test phase. Some of the fibers are broken or have poor transmission and alignment of the v-grooves is not very symmetrical. Fortunately only 19 of the 49 fibers are needed for the initial tests. The next fiber bundle should be much better given the lessons learned and the additional assembly fixtures planned.

The read noise of the CCID-35 system is bit higher than had been hoped but is within the ballpark to gather meaningful data. The plan is to address the read noise after completion of the first test phase.

The goal of the first test phase is to get a comparison of the WFS measurement variance and Strehl attenuation, as shown in the simulation plots, using the CCID-35 and APDs. Lab test and integration with PUEO are scheduled to continue through July with on-sky tests planned for some time mid-August 2006.

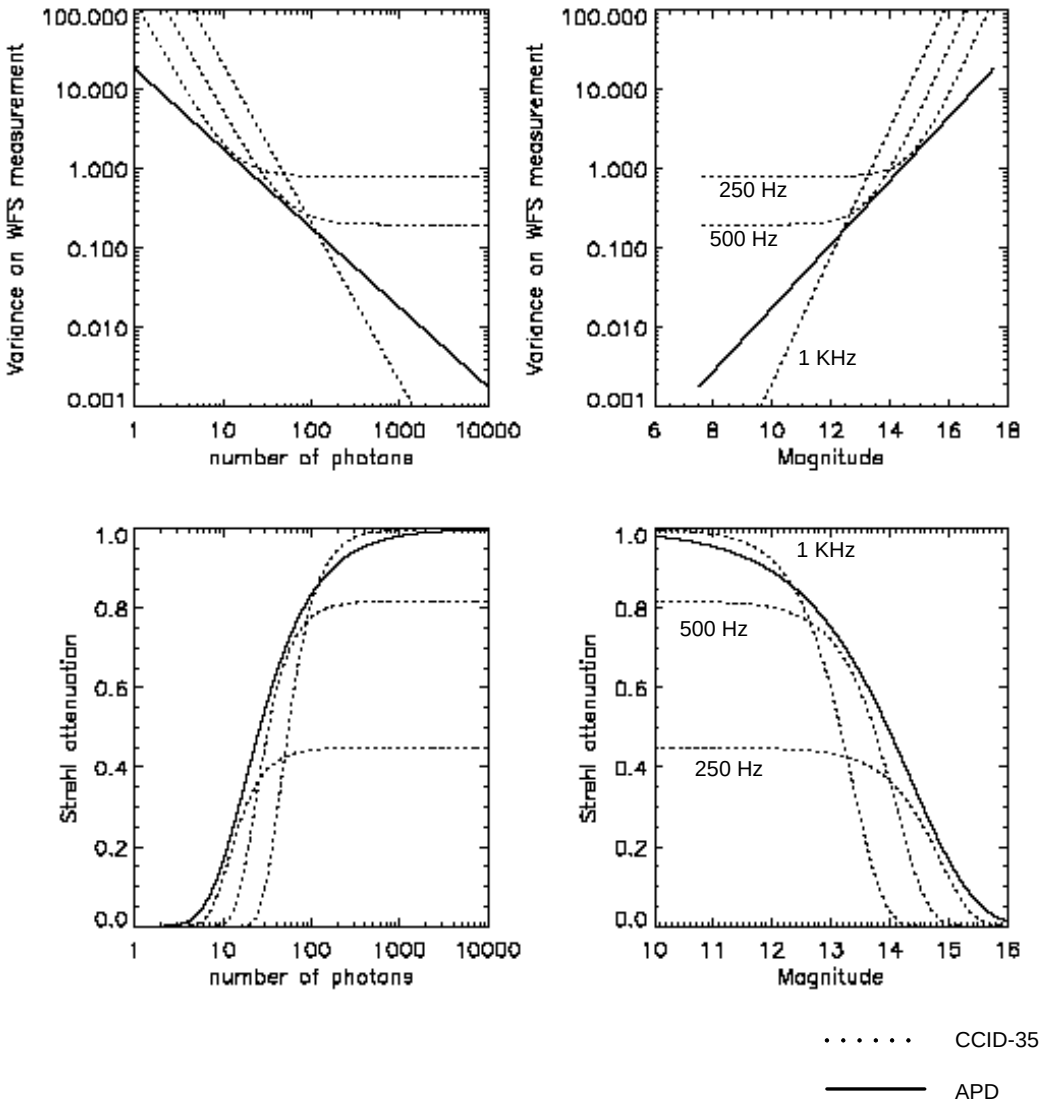

Figure 13 WFS measurement variance and Strehl attenuation.

REFERENCES

1. K. Ho, J.C. Cuillandre, P. Pascal, D. Salmon, O. Lai, J. Beletic, G. Luppino, R. Dorn, B. Burke, "Update report on FlyEyes – a dual CCD detector system upgrade for PUEO", *Proc. of SPIE, 5499*, pg 395, 2004.
2. J.C. Cuillandre, J. Beletic, R. Dorn, G. Luppino, S. Isani, N. Gorrcieix, O. Lai, T. Craven-Bartle, B. Burke, F. Menard, "FlyEyes: a dual CCD detector system for CFHT PUEO NUI's wavefront sensor", *Proc. of SPIE, 4839*, pg. 272, 2002.
3. R. Dorn, *A CCD based curvature wavefront sensor for Adaptive Optics in Astronomy*, PhD thesis, 2001.
4. J. Beletic, R. Dorn, T. Craven-Bartle, B. Burke, "A new CCD designed for curvature wavefront sensing", *Optical Detectors for Astronomy II*, Kluwer Academic Publishers, pg. 293, 2000.